Paper 039

TILT-ROTOR AERODYNAMICS ACTIVITIES DURING THE NICETRIP PROJECT

L. Vigevano[1], P. Beaumier[2], J. Decours[2], W. Khier[3], T. Kneisch[4], P. Vitagliano[5]

[1] Dipartimento di Scienze e Tecnologie Aerospaziali - Politecnico di Milano, Italy [2] ONERA, Meudon, France [3] DLR, Braunschweig, Germany [4] Airbus Helicopters, Donauwörth, Germany [5] CIRA, Capua, Italy

Abstract

The aerodynamic re-design and characterization of the Erica tilt-rotor aircraft, carried out by some Partners of the *NICETRIP* consortium, is presented. The re-design activities concern some specific aircraft components, like the fuselage/wing fairing, the wing airfoils, the blade cuff and the rotor spinner. The aerodynamic characterization is carried out both experimentally and numerically, although the present paper is focused on the numerical work, with the aim at identifying improvements of current ERICA geometry leading to improved aerodynamic performance.

1 Introduction

In recent years, the European rotorcraft industry has proposed the ERICA (Enhanced Rotorcraft Innovative Concept Achievement) tilt-rotor concept, aimed at high operational performance levels and characterized by: i)a small rotor diameter, to allow for conventional aircraft-mode take-off and landing; ii) a tiltable outer portion of the wing, to reduce the downwash effect in helicopter-mode; iii) a structural continuity of the rotor tilting mechanism, to increase the structural safety. The concept development has been partially funded by the European Commission through the 6^{th} framework project *NICETRIP*, which addresses the acquisition of new knowledge and technology validation related to the ERICA tilt-rotor full design process.

Within *NICETRIP*, the acquisition of the aerodynamic characteristics of the aircraft in the many different modes of operation was an important item. To this aim, both experimental and numerical activities have been carried out by a consortium of several Partners, formed by the research centers ONERA, DLR, NLR, CIRA, CENAERO, supplemented by Politecnico di Milano (PoliMi) and Airbus Helicopters Deutschland (AHD), formerly Eurocopter Deutschland (ECD). Two experimental models were designed and manufactured to assess the aircraft aerodynamic performances: a modular 1/8 model, non motorized, that was tested in the PoliMi large wind tunnel, and a highly sophisticated, motorized, 1/5 scale model that was tested in the DNW-LLF 9.5 $\times$ 9.5 m wind tunnel and in the ONERA S1MA wind tunnel. At the same time, CFD predictions were carried out to support the experimental findings and to complete the aerodynamic analysis. For the non powered model, an assessment of the prediction capabilities of the code employed was achieved, which led to the extrapolation of the measured results to account for Mach and Reynolds number effects. For the powered configuration, both pre-test and post-test simulations were carried out on different flight configurations.

The present paper attempts to summarize the numerical aerodynamic design and analysis activities performed during this seven-year long project. The paper is divided in two sections. The first section deals with the re-design of some aircraft components (i.e. the fuselage/wing fairing, the wing airfoils, the blade cuff and the rotor spinner) by means of CFD tools. The idea was to propose an upgrade of the basic configuration to be

tested during the project, but the modifications were not implemented in the experimental model because either they did not show a significant performance improvement or they were finalized too late in the project. Nevertheless, the achieved results constitutes an important source of information for future improvements of the aircraft design.

The second section deals with the aerodynamic characterization and the study of interference effects of the complete aircraft configuration by means of CFD tools. Both non powered and powered aircraft models were considered. The analysis of the non powered model is useful to assess the drag breakdown of the aircraft. The analysis of the powered model allows to assess the influence of the rotor wakes on the aerodynamic characteristics. Some flow interference effects were analyzed in detail, like the effect of the geometry of the wing-nacelle fairing. Pre-test calculations have been carried out to support the experimental campaigns and assess the influence of the model supports. Post-test simulations were carried out to carefully investigate the aircraft flow field both in airplane mode and conversion mode. A detailed comparison of the CFD results with the experimental data gathered in the DNW and S1MA wind tunnels for the motorized model is reported in another paper at this Conference[1].

2 Aerodynamic optimization

The aerodynamic re-design activities are summarized in the present section. Some of the activities did not lead to a geometrical modification of the aircraft, because the basic configuration was already performing fairly well. The optimization of the blade cuff and rotor spinner has allowed instead a substantial performance improvement.

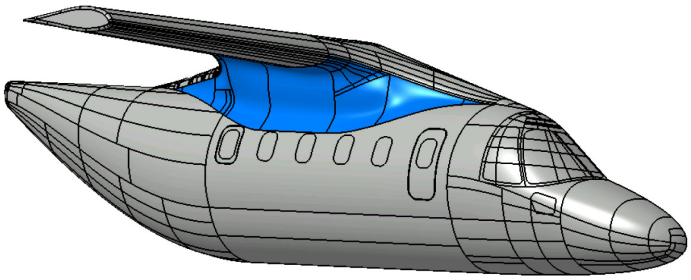

Figure 1: View of the simplified ERICA model. The zone to be optimized is highlighted in blue.

2.1 Fuselage/wing fairing shape optimization

The main objective of the re-design of the fuselage/wing fairing was the reduction of the drag, while keeping the lift at least equal to its baseline value. Some preliminary computations were performed on the complete ERICA non motorized configuration, with and without sponson, tail and nacelle, which verified that these elements do not noticeably influence the flow field near the fairing, thus allowing to carry out the optimization on the simplified geometry. The area to be optimized is highlighted in figure 1. The optimization chain used by CENAERO is made of four main blocks. The first one is a genetic algorithm optimizer, which receives the response variables from the RANS solver Argo and transmits the optimization parameters to the modeler. The modeler is made by the CAD system CATIA V5 and the tool providing the gateway to the geometry. The parametrization of the fairing shape was directly made under the CATIA V5 environment. CATIA is also responsible for the surface mesh of the model through its internal mesher FMS/FMD.

A geometry parametrization was created using three parameters acting respectively as thicknesses in the upper, central and lower parts of the fairing. The upper thickness turned out to be the most impacting parameter unlike the lower one which had nearly no influence on the outputs. The optimization results showed that digging into the fairing increases significantly the lift since the wing surface is increased. Because of that, the

induced drag increases accordingly. Conversely, when thickening the fairing, the lift decreases just as the drag until separation occurs downstream. Unfortunately, no improvement could be obtained on the drag while keeping the same level of lift. A 4.7% increase of the aerodynamic efficiency was obtained at the price of a 3.5% increase in drag. It was concluded that the baseline fairing geometry already performs fairly well and does not represent a significant part of the overall drag.

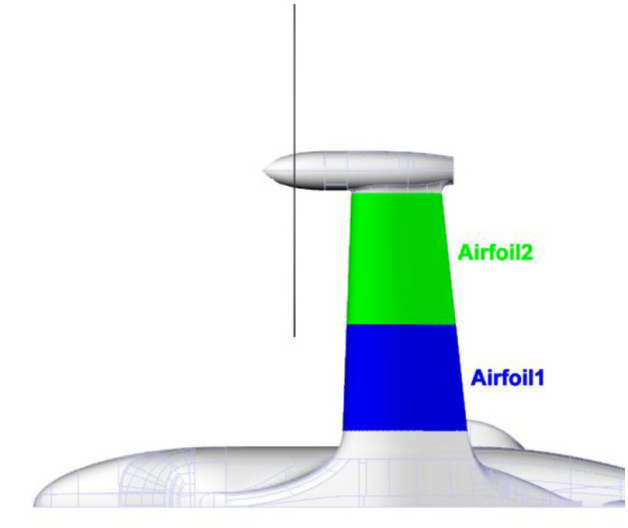

Figure 2: Wing flow regions

2.2 Wing airfoil optimization

The design goal for the wing sections optimization was again to reduce the aircraft drag at cruise flight condition. The rotor slipstream has an influence on the lifting surfaces and this effect has to be taken into account for the wing sections redesign. In fact, because of rotor slipstream, two different flow regions are identifiable on the wing, which are basically coincident with the fixed and tiltable parts of the wing, fig. 2.

The main analysis tools employed by CIRA to perform the optimization are a multi-objective genetic algorithm[2] and the Xload code, a quasi-3D fast analysis code which couples a vortex-lattice solver with Drela's MSES Euler/Boundary layer code[3]. By giving in input the analysis condition, the wing planform, the objective local lift coefficient and the dynamic pressure spanwise distribution along the wing – which accounts for the slipstream effect – Xload is able to generate an equivalent vortex-lattice mesh which has the same local load distribution as the original geometry. This equivalent vortex-lattice mesh is used to evaluate the local angle of attack distribution, which is the input for the MSES runs needed to calculate the local viscous drag coefficient. The optimization was carried out imposing as structural constraints the preservation of the native structure, the torsion tube dimensions and the fuel tanks capacity.

Multi-objective optimization led to the definition of two different optimal airfoils, the "laminar" Airfoil 76 for the inner wing and the "turbulent" Airfoil 18 for the outer part of the wing (fig. 3), whose aerodynamic characteristics are shown in figure 4, compared with those of the baseline airfoil. The analysis performed shows that only using the combination of Airfoil 76 for the inner part and Airfoil 18 for the outer part provides a sizeable drag reduction. In the inner part of the wing a viscous drag reduction around 20% is possible, but the geometry of the inner airfoil able to achieve this performance is quite different from the one of the section chosen for the outer wing. As a consequence, the junction has to be carefully designed in order to preserve the obtained performance improvement.

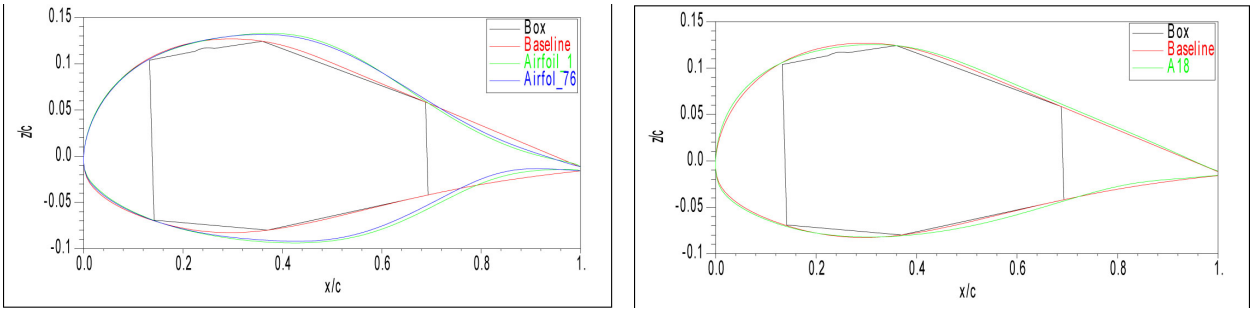

(a) Airfoil 76 (b) Airfoil 18

Figure 3: Airfoils 76 and 18 vs baseline geometry

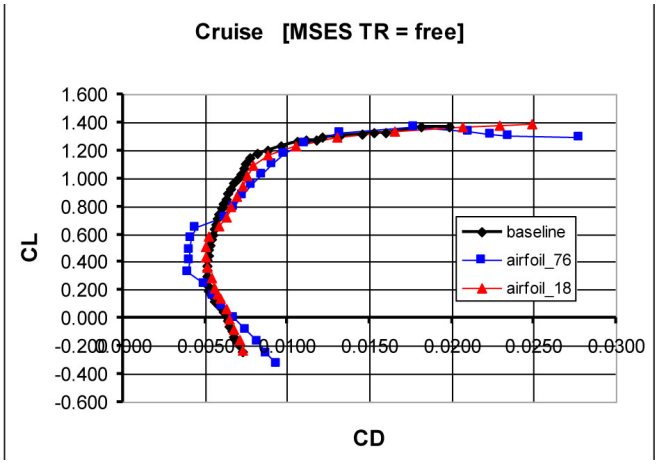

Figure 4: Modified airfoils polars at free transition

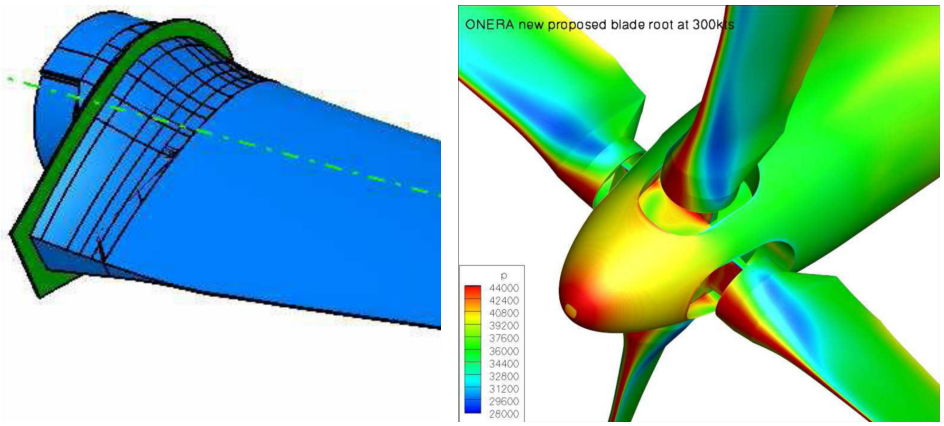

(a) AHD (b) Onera

Figure 5: Blade cuff geometry proposed by AHD and Onera

2.3 Blade cuff design

The blade cuff re-design was motivated by a modification of some structural constraints and by the observation of local flow separation regions at the blade root in cruise condition. Rather than using an automatic optimization method, the redesign was carried out by engineering judgement and CFD analysis.

Two blade root shapes satisfying the structural constraints have been proposed independently by AHD and ONERA (fig. 5), and performance has been evaluated both in hover and cruise. In hover condition the blade root design has a small impact on the propulsion system efficiency. Therefore, both AHD and ONERA blade roots present almost the same performance until the blade tip stalls. Both designs show also similar performance in cruise (fig. 6), with a 3% increase of the efficiency. Without any relaxation of the structural constraint it seems difficult to reach better performance in cruise. Only the modification of the aerodynamic part of the blade, aimed at limiting the loss of efficiency in the sweep law inversion region, could lead to performance improvement. On the other hand, computations performed by AHD with a new spinner design showed that a potential exists for the performance improvement of the complete propulsion system in cruise flight, as detailed in the next section.

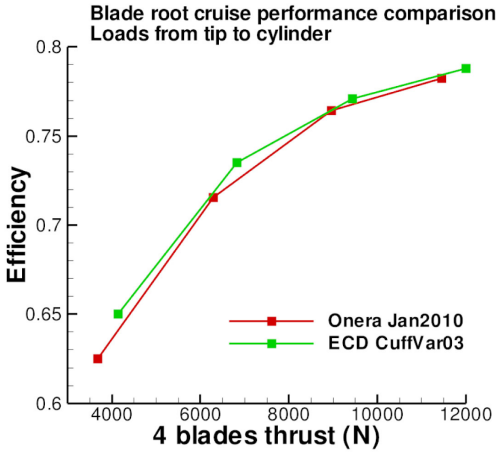

Figure 6: Cruise performance comparison between the geometries proposed by AHD (green) and Onera (red)

2.4 Rotor spinner design

Following a detailed performance breakdown of the cuff geometry, AHD proposed a new spinner geometry, designed to cover completely the yoke and a large part of the cylindrical root area thus minimizing the direct drag of these components (fig. 7). The modified spinner geometry has an important effect on the cylindrical part on the blade root – efficiency increased by about 4 counts – and on the yoke – efficiency increased by about 7.5 counts. The spinner shows no significant effect on the efficiency of the part of the rotor blade, which is outboard of the end plate.

A refinement of the spinner design was then performed by CIRA, using an aerodynamic optimization procedure based upon hybrid genetic algorithms and the ZEN URANS solver. The spinner shape was modified (fig. 8), by increasing the internal volume with respect to the baseline shape and preserving the diameter of the initial circular section, as required. The final analysis of the optimized configuration shows again that most of the improvement stems from a sort of shielding effect on the initial part of the blade cuff. It also suggests a significant effect of the cut-out fore rim position, in the sense that a larger improvement could be achieved by reducing the cut-out dimensions, particularly in front of the blade cuff. This would suggest to adopt some kind of flexible shroud to prevent the flow from entering inside the cavity, at least in front of the blade, while leaving the freedom of flapping motion.

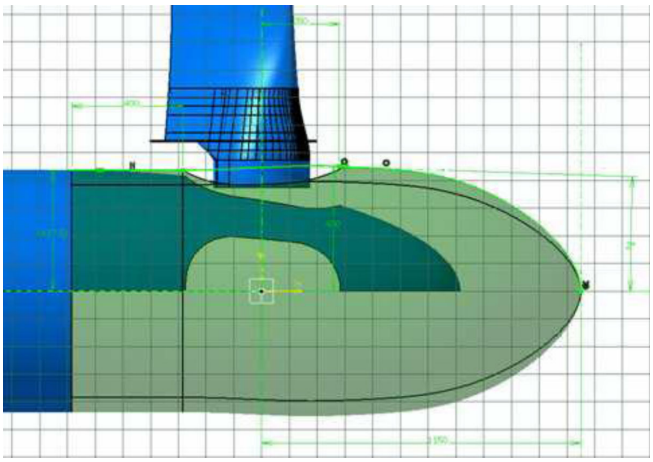

Figure 7: AHD spinner variant geometry

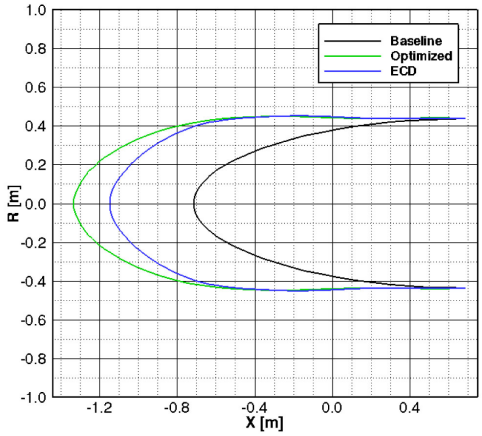

Figure 8: Shape of optimized spinner (green curve) compared with the baseline (black) and a modified shape initially proposed by AHD (blue)

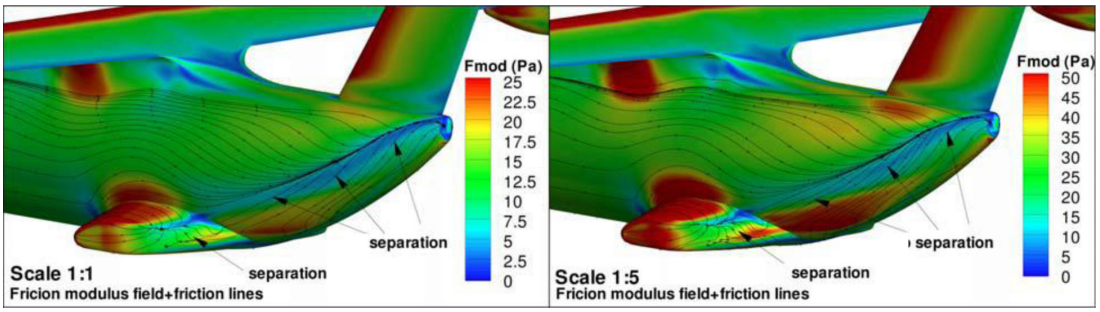

Figure 9: Flow topology and friction modulus (M=0.50, note that legend scales differ)

3 Aerodynamic analysis

3.1 Non powered model flow analysis

Three airplane mode operating conditions were selected for the numerical simulations of the non-powered model, at different aircraft speeds. All computations were performed with the ONERA code *elsA*[4], using Wilcox turbulence model with the Zheng limiter and the Kok diffusion correction.

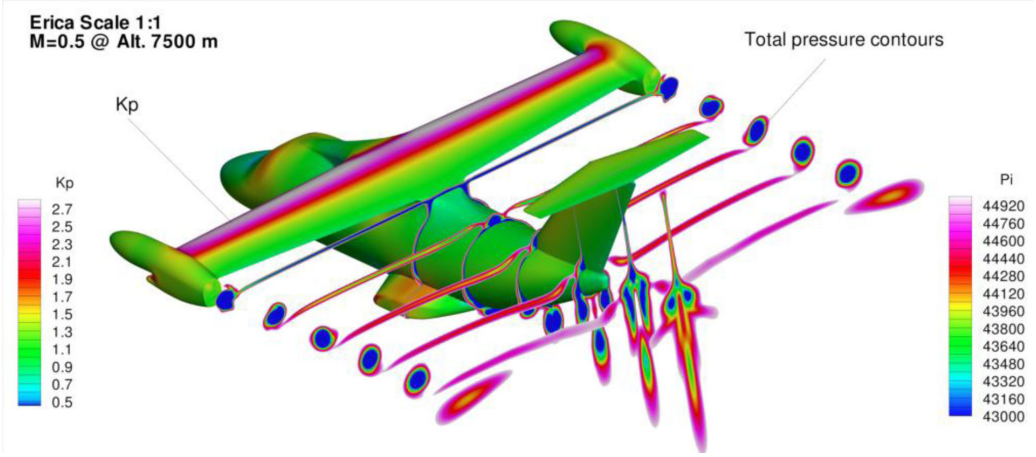

Figure 10: Scale 1:1 @ M=0.50: pressure coefficient and drag visualisation

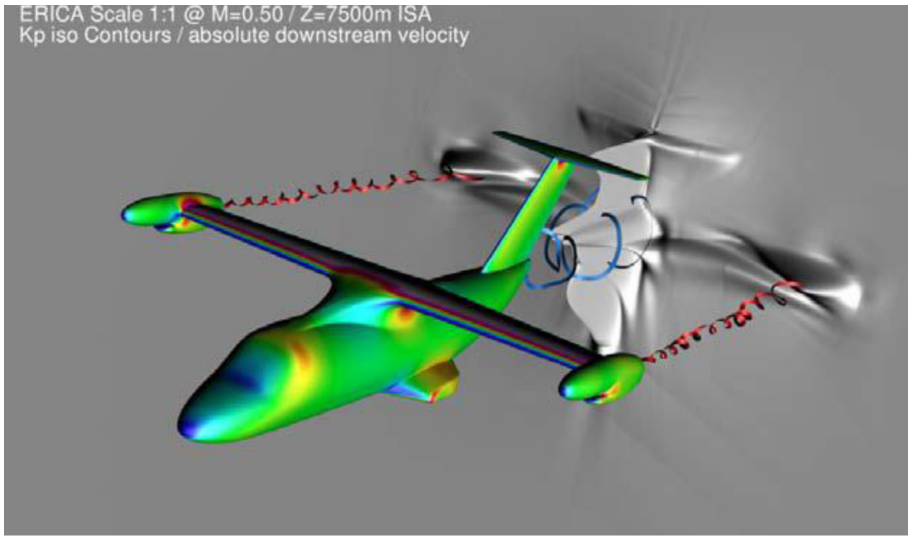

Figure 11: Scale 1:1 @ M=0.50: velocity defect downstream of the aircraft

The total number of cells is equal to 8.48×10^6 nodes for the half aircraft mesh. Calculations were performed for both full- and model-scale. At 1/1 scale they were carried out referring to the in flight operating conditions, while at 1/5 scale they were performed referring to the Modane S1MA tunnel conditions.

As the flow topology between scale 1/1 and scale 1/5 is similar, a detailed analysis of the flow is only made at scale 1/1. For both $M = 0.176$ and $M = 0.5$ symmetric cases, the flow is generally attached over most of the aircraft. Massive separated wakes are generated downstream of the nacelles and sponsons, see figures 9 and 10. A 3D separation line is observed in the rear part of the fuselage, which gives rise to well organized and rolled up vortex sheets in the near wake (fig. 10) that tend to merge close to the symmetry plane.

The aerodynamic coefficients are computed integrating the pressure and the friction stress over the aircraft skin (near-field approach). The normalized values of lift, drag and pitching moment coefficients at zero incidence are reported in Table 1 for different geometrical scales and Mach numbers. The rightmost column shows the results of a calculation performed with a steady, uniform Actuator Disk (AD) model.

As expected, the Reynolds number effect, given by the comparison between scale 1/1 and scale 1/5 results, is to increase the drag and to

decrease the lift. The main effect of Mach number is to increase the lift coefficient following the Prandlt-Glauert correction. The effect of the rotor, modeled as an AD, on the global loads appears to be very limited. The comparison with the wind tunnel test provided by PoliMi is rather good when remaining below 5 deg angle-of-attack. At higher incidence the computations overestimate the maximum lift and drag.

The near-field technique is the classical method to assess the lift and drag of a body. This approach is however known to be reliable for lift but not always for drag. To compute the drag more accurately, the far-field technique can be employed[5], which relies on the momentum theorem and mass conservation laws and takes advantage of the calculation of the velocity defect (fig. 11). In addition, the far-field analysis may give the drag breakdown, separating viscous, wave and lift-induced drag. The difference between the near-field and the far-field drag is the so-called spurious drag. The far-field analysis of the present cases shows that the spurious drag is equal to 16 drag counts for both the 1/1 and 1/5 scales. As the Mach number, the numerical scheme, the mesh and all numerical parameters are unchanged, this spurious drag remains remarkably constant and represents about 3% of the total drag. Although this level of spurious drag is higher than what is found in conventional fixed wing applications, this figure quantifies the accuracy of the near-field approach and thus increases the confidence of the presented results.

Geometrical scale	1/5	1/5	1/1	1/1	1/1	1/1
M	0.176	0.5	0.176	0.5	0.55	0.5 (with AD)
Lift coeff.	0.959	1.090	1.0	1.1195	1.162	1.128
Drag coeff.	1.191	1.516	1.0	1.0905	1.127	1.0805
Pitching mom. coeff.	0.949	1.076	1.0	1.1105	1.1475	1.1185

Table 1: Normalized aerodynamic coefficients in airplane mode at zero angle-of-attack, non powered model

3.2 Wing/nacelle fairing effects

During the TILTAERO program it was shown by numerical simulations that flow separation occurs on the tiltable wing, close to the wing/nacelle fairing, during the conversion phase. Within the NICETRIP program, additional geometries have been tested by Onera in the attempt of limiting the loss of lift due to the nacelle and tiltable wing flow separation. The main geometry modification consists in the addition of a simple end plate on the tiltable wing suction side, from the stagnation point to the trailing edge (fig. 12).

Navier-Stokes computations were run with ONERA code *elsA* with AD. Representative results for the high-speed case TP4 (nacelle tilt angle of 60 deg, fixed wing angle of attack of 3 deg and movable wing pitch of 3.7 deg; rotor thrust of 3700N and wind velocity equal to 57.1m/s) are shown in figure 13. Strong aerodynamic interactions appear at the nacelle-wing fairing. For the original geometry these interaction effects generate flow separation on the outer wing at all different flight configurations considered. The simple end plate has shown good performance and stability improvement capabilities at low speed flight, but is not sufficient for medium and high speed conversion configurations. The same end plate combined with the suppression of the wing-nacelle fairing geometry has shown remarkable ability to reduce the flow separation at very low speed and suppress it in medium and high speed configurations. This leads to important aerodynamic performance improvement, in terms of lift (fig. 14) and drag forces in addition to significant stability increase.

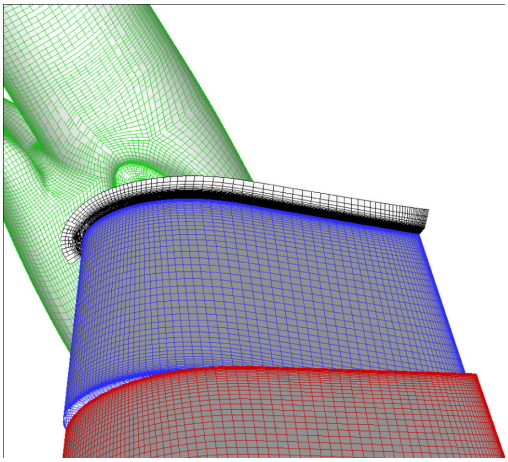

Figure 12: End plate geometry on the tiltable wing.

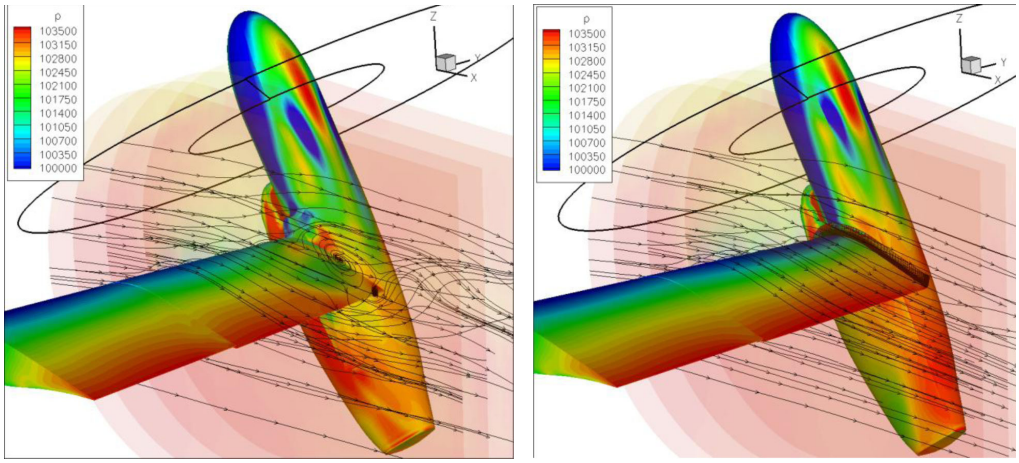

(a) original geometry (b) end-plate geometry

Figure 13: Flow field at the wing/nacelle fairing

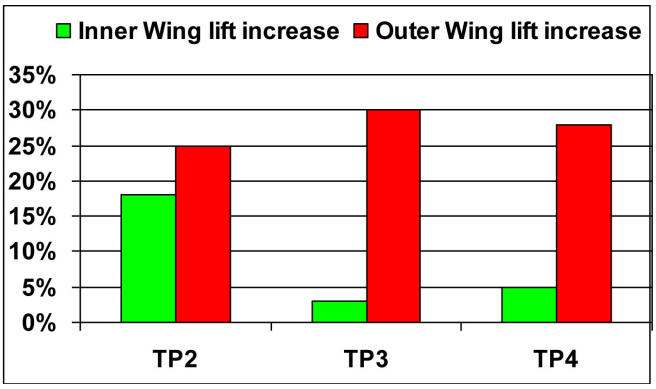

Figure 14: Lift increase with the end plate and without the nacelle-wing junction

3.3 Powered model pre-test analysis

The results presented and discussed in this and the following section are based on the time-accurate solution of the Unsteady Reynolds Averaged Navier-Stokes (URANS) equations in three dimensions by means of three CFD block-structured, finite volume codes: *elsA*[4] by ONERA, *FLOWer*[6] by DLR and AHD, and *ROSITA*[7] by PoliMi, all based on a cell-centered finite volume spatial discretization on multi-block structured grids and moving Chimera techniques, but differing with respect to, mainly, turbulence models.

The 1/5 powered model pre-test results were discussed in detail elsewhere[8] and only a concise summary will be repeated here for completeness. DLR and AHD generated overlapping grid sets for the lower support configuration to be tested in the $9.5 \times 9.5\,m^2$ test section of the DNW-LLF wind tunnel, while ONERA and PoliMi cooperated in generating an overlapping grid assembly for the rear-support configuration to be tested in the $8\,m$ diameter circular test section of the S1MA wind tunnel. The resulting grids have similar dimensions, ranging from 22.5×10^6 to 19×10^6 nodes. A slightly smaller grid (17.7×10^6) was used with an AD model by AHD. DLR and AHD grids present a slightly less refined surface discretization than ONERA/PoliMI grid; the latter has also a better representation of the blade root, which has proven to be important to correctly represent the flow over the nacelle, but does not influence the loads on the lifting part of the blade. All calculations refer to the airplane mode configuration ERICA model installed in the wind tunnel at 0 deg incidence.

Global loads on the tiltable wing show a noticeable 4/rev lift distribution accounting for the blade rotation, with average lift values of the time-accurate computations being within +/- 10% to the steady AHD value.

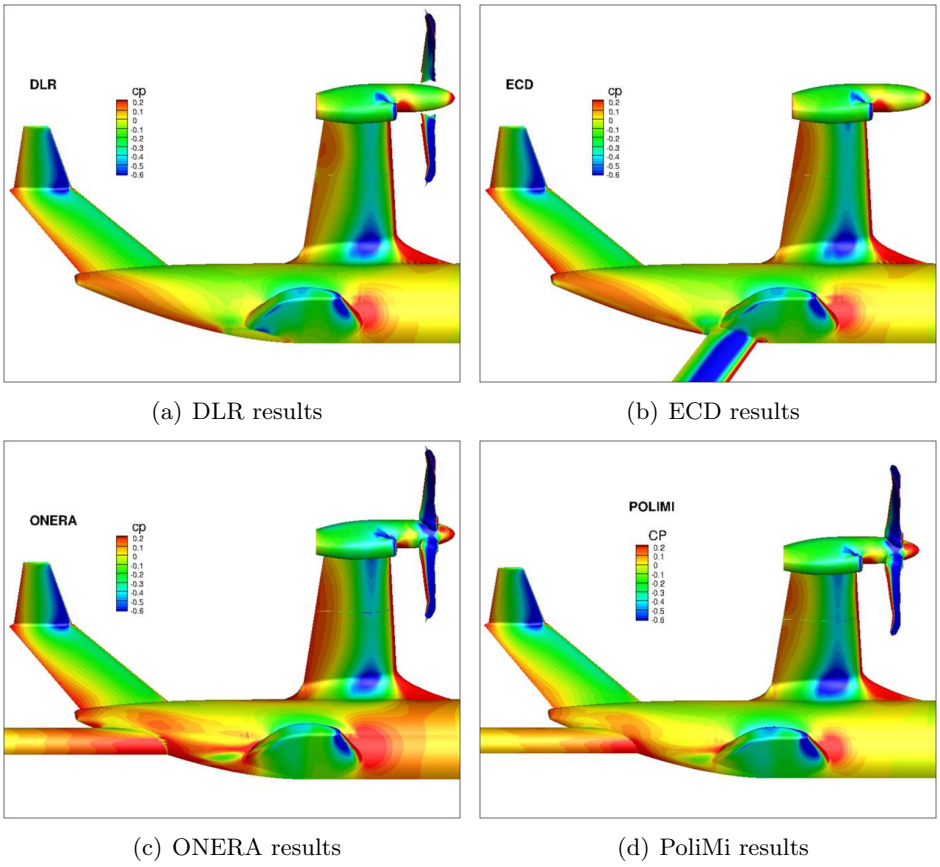

(a) DLR results (b) ECD results

(c) ONERA results (d) PoliMi results

Figure 15: Pressure field on aft part of the fuselage

The effect of the presence of the blade root in the calculations reduces noticeably the lift contribution of the nacelle.

The pressure distribution on the front part of the fuselage is quite similar for all computations, implying a small influence of the type of support. Note that the support is not depicted in the DLR results although present in the simulation. The local influence of the lower-mounted support is overall very limited in the DLR and AHD calculations, while larger effects are produced by the rear-mounted support in the ONERA and PoliMi calculations (see fig. 15). Notwithstanding a rather good qualitative comparison of the pressure distributions, the quantitative lift coefficient in fig. 16(a) shows different behaviors. The rear-mounted support configuration introduces a higher degree of unsteadiness of the global fuselage loads. Comparison between DLR and AHD results allow to state that the influence of the rotor model on the fuselage pressure is almost negligible in this airplane mode configuration, since the AD calculations gives the same pressure distribution as the fully unsteady calculations. They also produce similar results for the lift coefficient. Some quantitative differences are found instead in the drag coefficient values (fig. 16(b)).

The pressure distributions on the outer, lifting part of the blade show a remarkable qualitative agreement among all computations.The large variation of thrust generated by a single blade during one rotor revolution, shown in figure 17 is generated by the strong induced velocity field of the tiltable wing.

From the analysis of the pre-test computed results, it can be concluded that the overall qualitative agreement of the pressure distributions among different calculations is somewhat acceptable, while the scatter of the quantitative average loads is still important.

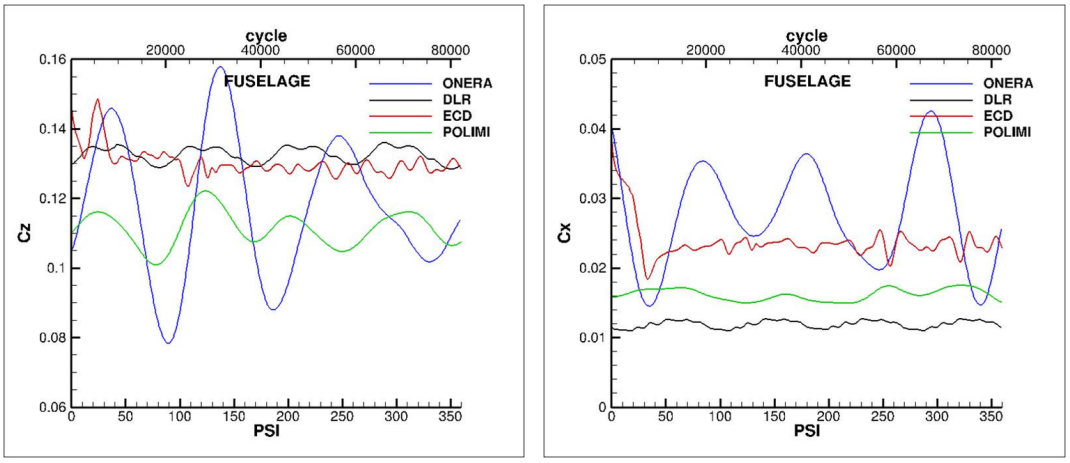

(a) Cz (b) Cx

Figure 16: Global loads on the fuselage

3.4 Powered model post-test analysis

Among the several operating conditions that were tested in the DNW-LLF and ONERA S1MA wind tunnels, four configurations were selected for the post-test calculation phase, namely one aircraft mode at high incidence, labeled AC1, and three conversion-corridor mode configurations, referred to as CC1, CC2 and CC4. Details of the selected configurations, in terms of geometrical setting and operating conditions, are given in Table 2.

Due to the lack of space, we limit ourselves to summarize the conclusions of the comparison exercise, referring to another paper at this Conference[1] for a detailed analysis of the achieved results.

For the high-incidence configurations considered, the flow over the aircraft fuselage and wing presents large separation regions. The numerical prediction of these separation regions is very much influenced by the turbulence model employed, or more precisely by the combination between grid

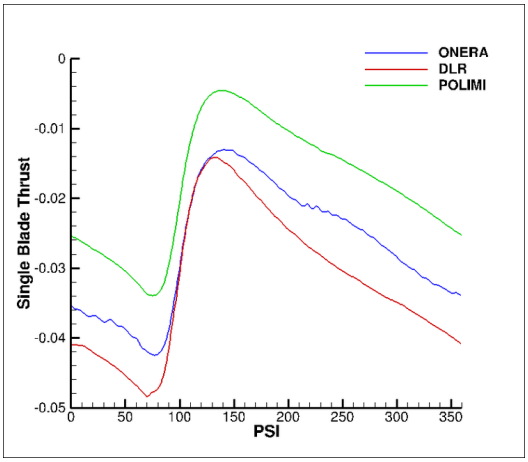

Figure 17: Thrust coeff. on the rotor blade

and turbulence model. As an example, figure 18 shows the pressure field and the limiting streamlines for the AC1 case: while ONERA and AHD calculations, using different versions of the $k-\omega$ model, predict a large separation region on the wing fuselage junction, close to the aircraft centerline, PoliMi (Spalart-Allmaras) and DLR ($k-\omega$) calculations predict a strong influence of the flow through the wing gap, causing a large separation on the wing, and a very limited or no separation at all at the centerline. The presence of the separation region close to the centerline can be deducted from the experimental pressure distribution along the aircraft upper surface, at the centerline, as shown in figure 19. Due to the differences in the flow field predictions, also the quantitative loads calculations differ among the Partners.

	α [deg.]	θ_{tiltw} [deg.]	θ_{nac} [deg.]	Mach	Re $\times 10^{-6}$
AC1	9.9	0.0	0.0	0.17	1.94
CC1	4.1	30.5	77.8	0.09	1.02
CC2	2.4	6.7	61.8	0.14	1.65
CC4	5.3	4.1	30.0	0.17	1.95

Table 2: Description of the considered aircraft configurations, in terms of fuselage incidence, tiltable wing and nacelle inclinations and operating conditions.

4 Conclusions

This work summarizes the numerical aerodynamic activities performed during the *NICETRIP* project, which mainly consist of the aerodynamic characterization of the Erica tilt-rotor aircraft and a partial re-design of some of its components, i.e. the fuselage/wing fairing, the wing airfoils, the blade cuff and the rotor spinner.

The design modifications proposed for the fuselage/wing fairing and the wing airfoils showed no significant performance improvement with respect to the baseline design. A sizeable improvement for the aircraft flying in airplane mode was instead demonstrated with the re-design of the blade cuff and the rotor spinner. The introduction of an end plate on the tiltable wing was also shown to reduce considerably the wing/nacelle interference effects. We were not able to confirm these findings experimentally, because the modifications were not implemented in the experimental model used during the wind tunnel tests. Nevertheless, the achieved results constitutes an important source of information for future improve-

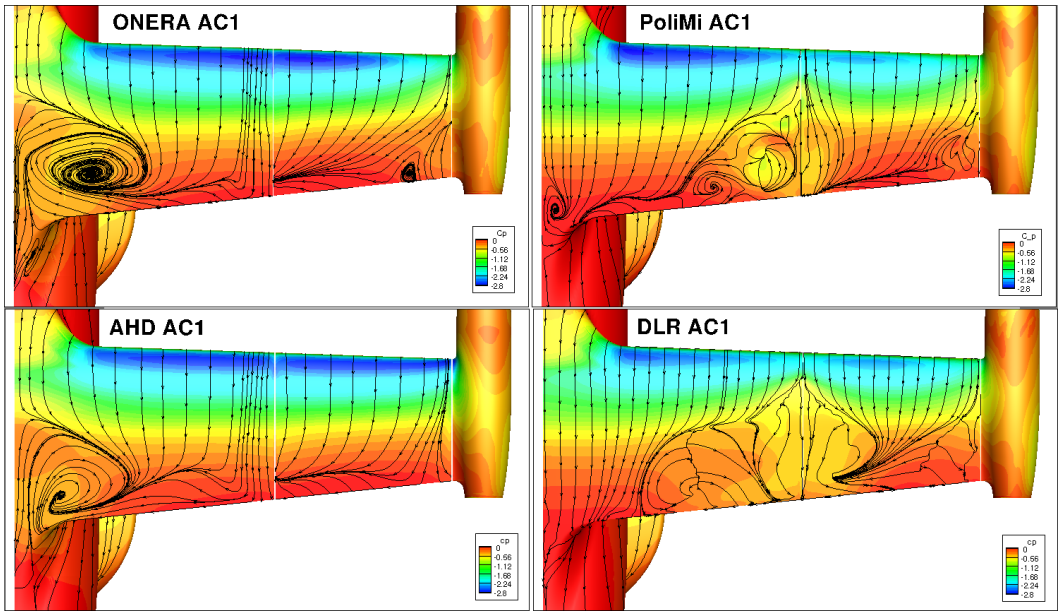

Figure 18: Pressure field and limiting streamlines on the upper surface of the aircraft. AC1 case.

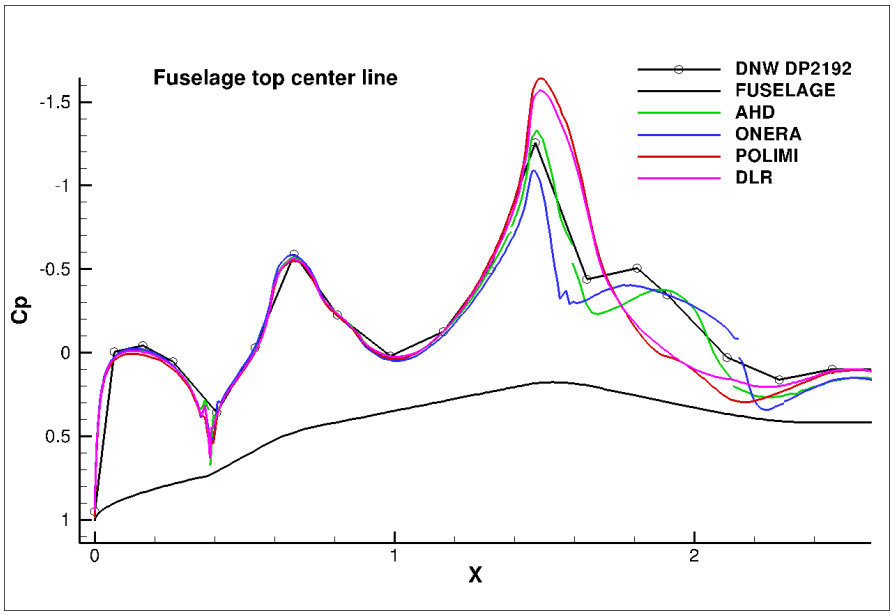

Figure 19: Comparison with the experimental pressure distribution along the centerline on the upper surface of the aircraft. AC1 case.

ments of the aircraft design.

The aerodynamic characterization of the Erica aircraft has been carried out for both the non powered and powered models, in parallel with the experimental investigations. The simulations of the non powered configuration put confidence on the drag breakdown analysis, carried out experimentally. Furthermore, they allowed to quantify the Reynolds and Mach number effects and to shed light on the flow features responsible for the larger sources of drag.

Blind-test numerical predictions in airplane mode were carried out by some Partners of the *NICETRIP* consortium, i.e. ONERA, DLR, AHD and PoliMi. The calculations were carried out with different codes, different turbulence models, different wind tunnel setups and different grids, with the objective of supporting the experimental test campaigns in the DNW-LLF and ONERA S1Ma wind tunnels. From the blind-test prediction it was concluded that time-accurate calculations are required, because the unsteadiness introduced by the rotor wake on the aerodynamic loads on the fuselage, wing and nacelle may be relevant. The influence of the lower-mounted wind tunnel support used in the DNW tunnel was shown to be rather limited, while the rear-mounted support used in the S1Ma tunnel introduces some local unsteady effects on the fuselage loads. The overall qualitative agreement of the pressure distributions among different calculations was found acceptable, while the scatter of the quantitative average loads is still important.

The post-test predictions were focussed on high-incidence operating conditions, that represent a difficult test case. The compared calculations differ for both grid characteristics and turbulence model employed. A significant scatter of results was found, which indicates that for highly separated flows the accuracy of the present predictions methods is still heavily dependent on a wisely selected combination of grid characteristics and turbulence model choice.

Aknowledgements: this work has been partially funded under the EC supported FP6/Aeronautics Project AIP5-CT-2006-03-944 *NICETRIP*.

References

[1] J. Decours, P. Beaumier, W. Khier, T. Kneisch, M. Valentini, and L. Vigevano. Experimental validation of tilt-rotor aerodynamic predictions. In 40^{th} *European Rotorcraft Forum, Southampton, U.K.*, 2014.

[2] A. Vicini and D. Quagliarella. Inverse and direct airfoil design using a multiobjective genetic algorithm. *AIAA J.*, 35:1499–1505, 1997.

[3] M. Drela. Newton solution of coupled viscous/inviscid multielement airfoil flows. In *AIAA Fluid Dynamics, Plasma Dynamics and Lasers Conference, Seattle, WA. AIAA 90-1470*, 1990.

[4] L. Cambier, S. Heib, and S. Plot. The ONERA elsA CFD software: input from research and feedback from industry. In 28^{th} *Congress of the International Council on the Aeronautical Sciences, Brisbane*, 2012.

[5] S. Esquieu. Reliable drag extraction from numerical solutions: Elimination of spurious drag. In *NATO Symposium AVT 147, Athens, Greece*, 2007.

[6] N. Kroll, B. Eisfeld, and H.M. Bleecke. The Navier-Stokes Code FLOWer. In *Notes on Numerical Fluid Mechanics, Vieweg, Braunschweig*, volume 71, pages 58–71, 1999.

[7] M. Biava. *RANS computations of rotor/fuselage unsteady interactional aerodynamics*. PhD thesis, Dipartimento di Ingegneria Aerospaziale, Politecnico di Milano, 2007.

[8] L. Vigevano, M. Biava, P. Beaumier, J. Decours, W. Khier, and T. Kneisch. Code to code comparison of aircraft-mode tilt-rotor aerodynamics. In 38^{th} *European Rotorcraft Forum, Amsterdam, the Netherlands*, 2012.